



Promoting austenite formation in laser welding of duplex stainless steel—impact of shielding gas and laser reheating

Amir Baghdadchi¹ · Vahid A. Hosseini¹ · Kjell Hurtig¹ · Leif Karlsson¹

Received: 10 September 2020 / Accepted: 3 November 2020 / Published online: 9 November 2020
© The Author(s) 2020

Abstract

Avoiding low austenite fractions and nitride formation are major challenges in laser welding of duplex stainless steels (DSS). The present research aims at investigating efficient means of promoting austenite formation during autogenous laser welding of DSS without sacrificing productivity. In this study, effects of shielding gas and laser reheating were investigated in welding of 1.5-mm-thick FDX 27 (UNS S82031) DSS. Four conditions were investigated: Ar-shielded welding, N₂-shielded welding, Ar-shielded welding followed by Ar-shielded laser reheating, and N₂-shielded welding followed by N₂-shielded laser reheating. Optical microscopy, thermodynamic calculations, and Gleeble heat treatment were performed to study the evolution of microstructure and chemical composition. The austenite fraction was 22% for Ar-shielded and 39% for N₂-shielded as-welded conditions. Interestingly, laser reheating did not significantly affect the austenite fraction for Ar shielding, while the austenite fraction increased to 57% for N₂-shielding. The amount of nitrides was lower in N₂-shielded samples compared to in Ar-shielded samples. The same trends were also observed in the heat-affected zone. The nitrogen content of weld metals, evaluated from calculated equilibrium phase diagrams and austenite fractions after Gleeble equilibrating heat treatments at 1100 °C, was 0.16% for N₂-shielded and 0.11% for Ar-shielded welds, confirming the importance of nitrogen for promoting the austenite formation during welding and especially reheating. Finally, it is recommended that combining welding with pure nitrogen as shielding gas and a laser reheating pass can significantly improve austenite formation and reduce nitride formation in DSS laser welds.

Keywords Duplex stainless steel · Laser welding · Shielding gas · Laser reheating · Austenite fraction

1 Introduction

Duplex stainless steels (DSS), with a nearly equal amount of ferrite and austenite, have received much attention in recent years, thanks to offering both high corrosion resistance and superior mechanical properties [1]. In DSS, a balanced phase fraction is of vital importance as the best combination of mechanical properties and corrosion resistance comes by approximately equal fractions of ferrite and austenite [2].

Laser welding has the potential to accelerate the fabrication of components [3, 4]; however, some metallurgical challenges

limit its applications in DSS. Solidification of DSS is fully ferritic and followed by the diffusion-controlled solid-state ferrite to austenite transformation. Rapid cooling, when using low-energy input processes such as laser welding, restricts the austenite formation and disturbs the optimum phase balance in DSS. This condition also increases the risk of nitride formation due to the supersaturation of nitrogen in ferrite. It may, therefore, deteriorate the corrosion properties and toughness of DSS laser welds [5, 6]. Nitrogen content is of great importance in promoting austenite formation, especially during autogenous welding [7, 8], as it has a high diffusion rate and is a strong austenite former [9, 10]. Nitrogen loss will, therefore, limit the austenite formation during welding of DSS [11]. The decrease of nitrogen content is not restricted to the weld metal (WM); the heat-affected zone (HAZ) is also influenced by nitrogen diffusion from the HAZ to the WM [12–14].

In recent years, the effect of shielding gas on welding of DSS, as one of the most important factors of controlling weld properties, has been studied [15–17]. Table 1 presents laser welding parameters, information about base material,

Recommended for publication by Commission IX - Behaviour of Metals Subjected to Welding

✉ Amir Baghdadchi
amir.baghdadchi@hv.se

¹ Department of Engineering Science, University West, SE-461 86 Trollhättan, Sweden

Table 1 Laser welding parameters, base material characteristics, shielding gas, and austenite fraction in laser welding of DSS

	Base material		Laser method	Power (W)	Welding speed (mm/s)	Energy input (J/mm)	Shielding gas	Backing gas	Austenite Fraction (%)
	Steel	Nitrogen content							
Yang et al. [18]	2205	0.17	Not reported	1500	33	45	Ar	Ar	7
Westin et al. [19]	LDX 2101	0.21	Fiber	5000	50	100	Ar	Ar	13
	LDX 2101	0.22	Disc	2000	83	80	Ar	Ar	17
Karlsson et al. [5]	2507	0.26	Nd:YAG	4000	17	240	Ar	–	22
	2205	0.16	Fiber	3000	10	300	Ar	N ₂	25
Westin et al. [19]	LDX 2101	0.23	Nd:YAG	1000	50	20	N ₂	Ar	19
	2205	0.17	CO ₂	5600	35	160	N ₂	–	24
Capello et al. [22]	LDX 2101	–	Disc	2000	25	80	N ₂	N ₂	29
	2205	0.16	Fiber	3000	10	300	N ₂	N ₂	41
Lai et al. [21]	LDX 2101	0.25	CO ₂	5000	66	80	He	Ar	42

shielding gas, and the resulting austenite fraction in laser welding of DSS in different studies. Salminen et al. [23] argued that a higher content of nitrogen in the shielding gas leads to an increase in austenite fraction of 2205 DSS laser welds. Keskitalo et al. [20], during laser welding of LDX 2101 DSS, observed that by replacing argon with nitrogen as shielding gas, the austenite fraction increased from 17 to 29%, thanks to a higher nitrogen content of the WM with nitrogen shielding. Lai et al. [21] also reported an increment of austenite fraction from 25 to 41% by changing from argon to nitrogen shielding gas in laser welding of 2205 DSS. It should be noted that other laser welding parameters such as laser type, power, speed, and focus spot size as well as the DSS grade and its thickness are as important as the choice of shielding gas for the final austenite fraction of the weld metal. The highest austenite fraction reported in Table 1 was, for example, reported for CO₂ laser welding of thin LDX 2101 with He as shielding gas which cannot directly be explained by nitrogen promoting austenite formation.

Reheating or heat treatment is another approach employed to promote austenite formation in DSS laser welds. Heat treatment after welding has been employed in several studies to increase the time available for ferrite to austenite transformation [18, 22, 24–26]. Saravanan et al. [24] improved the austenite fraction of 2507 DSS laser welds about 12% by post-weld heat treatment (PWHT) at 1050 °C for 2 h in a furnace. Young et al. [25] also reported that 60-min furnace PWHT at 1050 °C increased austenite fraction from 25 in as-welded condition to 55%. In another study, Yang et al. [18] showed that furnace PWHT at 1080 °C for 3 min increased austenite formation from 7 in as-welded condition to 54%. Despite that furnace PWHT promotes the austenite formation, it may not be feasible for large and/or complex geometries, and it may significantly increase the production time. Capello et al. [22] used laser heat treatment, as an alternative method to furnace heat treatment, to promote austenite formation in DSS welds. They successfully showed the possibility of laser reheating to increase the austenite fraction in DSS welds. However, they found a heterogeneous microstructure in the weld with a high fraction of secondary austenite in the top with no significant increase of austenite content in the bottom. Kolenic et al. [27], moreover, increased the austenite fraction of 2507 SDSS laser welds using defocused laser beam reheating. However, a lower amount of austenite was achieved in the root compared to the surface and center of the welds due to relatively low peak temperatures and the use of argon shielding gas.

Despite the need from the industry, no special guidelines are available to advise on the combined effect of the choice of shielding gas and laser reheating when aiming at maximizing the austenite formation with a minimum delay in the production time of autogenous DSS laser welding. In practice, it is often challenging to reach an acceptable phase balance with less than 70 vol.% of ferrite during autogenous laser welding

of DSS. Therefore, the present study aims at finding practical ways of improving austenite formation through the selection of a suitable shielding gas and if needed combined with laser reheating. The influence of shielding gas, pure argon and pure nitrogen, and laser reheating was investigated in laser welding of 1.5-mm thick FDX 27 DSS using light optical microscopy complemented with thermodynamic calculations. The FDX 27 DSS is a relatively new alloy designed to improve the formability of DSS, where the influence of welding on microstructure and properties has been little studied. The specific characteristics of FDX 27 DSS such as high ductility and formability rely on the transformation-induced plasticity effect [28, 29], requiring a sufficient austenite fraction. Hence, ensuring sufficient formation of austenite during laser welding is of great importance to expand the range of possible applications of this grade.

2 Material and method

2.1 Material and welding/reheating

In this study, 1.5-mm-thick FDX 27 (UNS S82031) lean DSS sheets were welded and reheated by autogenous laser welding. The chemical composition of the base material is given in Table 2.

A schematic illustration of the welding and reheating passes is shown in Fig. 1. An IPG Photonics YLR-6000 fiber laser was used for both welding and reheating. The welding was carried out with 2700-W laser power and a welding speed of 30 mm/s. The focal lengths of the collimating lens and focusing lens were 120 mm and 200 mm, respectively. The fiber diameter was 600 μm , which produced a spot size of 1 mm on the plate surface. In reheating, while the optics were the same as for welding, the power and the welding speed were 550 W and 9 mm/s, respectively. In addition, the laser beam focus was positioned 50 mm above the surface for reheating passes. To investigate the effect of shielding gas on both welding and reheating, either pure argon (100%) or pure nitrogen (100%) was used as both shielding and backing gas for welding and reheating. In the trailing shielding, the shielding gas was maintained behind the laser and protected the WM until it cooled down below approximately 100 $^{\circ}\text{C}$. The thermal cycles of welding and reheating passes were recorded by a thermocouple located on the backside of the sheet,

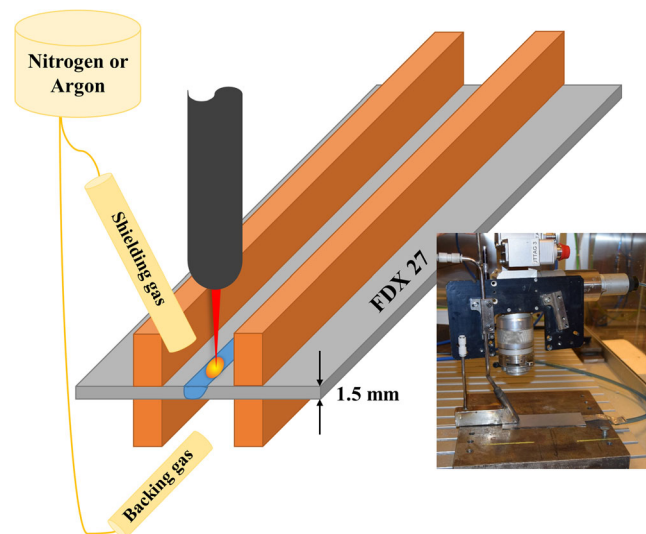


Fig. 1 Schematic illustration and photo of the laser welding set-up and configuration of gas protection by trailing shielding and backing gas

approximately 1.5 mm from the fusion zone. The four welded samples are denoted as follows: Ar-as-welded, N_2 -as-welded, Ar-reheated, and N_2 -reheated which refer to Ar-shielded welding, N_2 -shielded welding, Ar-shielded welding followed by Ar-shielded laser reheating, and N_2 -shielded welding followed by N_2 -shielded laser reheating, respectively.

2.2 Microstructure analysis

Cross-sections of the as-welded and reheated samples were ground, polished, and etched with modified Beraha reagent (60 ml water, 30 ml HCl, 0.6–0.7 g potassium bisulfite) for 12–15 s [30]. A Zeiss Axio Imager.M2m optical microscope was used to study the microstructures in both WM and HAZ. The phase balance was measured by image analysis (IA) using Image-Pro-9.2 software.

2.3 Estimation of nitrogen content

Measuring the nitrogen content of the WM with direct methods was not feasible in this study. The extraction of samples with a sufficient volume for LECO analysis by drilling was not suitable due to the very narrow weld zone. Nitrogen measurement using wavelength dispersive x-ray spectrometry (WDS) was not expected to be accurate with the available methodology, as in a recent study, Hosseini et al. [12] obtained very scattered data with significantly lower values for nitrogen content (0.08–0.20% N) compared to that in the material certificate (0.27% N) for 2507 super DSS base metal. The nitrogen content of the WM was, therefore, estimated with an indirect method. In this technique, the 1.5-mm-thick and 30-mm-wide as-welded samples were subjected to a 2-min heat treatment

Table 2 Chemical composition of the base material

	C	Si	Mn	P	S	Cr	Ni	Mo	Cu	N
FDX 27	0.03	0.42	1.09	0.024	0.001	20.0	2.8	1.20	0.33	0.186

in vacuum at 1100 °C in a Gleeble 3800 thermo-mechanical simulator, to reach a near-equilibrium condition. In the following quenching, the water-cooled grips reduced the temperature from 1100 to 800 °C in less than 4 s which is judged to be sufficiently fast to avoid significant changes in the phase fraction. In the next step, the austenite fractions of the heat-treated samples were measured by image analysis. Then, the ferrite and austenite fractions were calculated by the Thermo-Calc version 8.5.1.0017 software with the TCFE10 database at 1100 °C for nitrogen contents from 0 to 0.2 wt.%. In the final step, WM nitrogen content was estimated by comparing the obtained phase fraction after Gleeble heat treatment and the phase diagram calculated with Thermo-Calc.

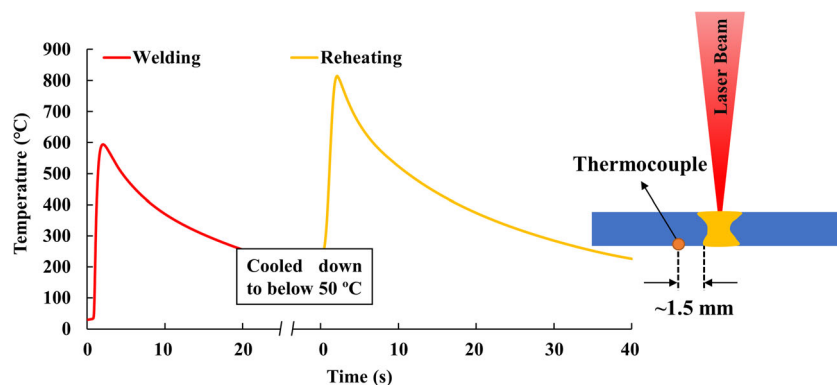
3 Results

3.1 Weld profile and thermal cycles

The thermal cycles recorded by the thermocouple and its schematic location are shown in Fig. 2. There are two peak temperatures, where the first one is for the welding pass and the second one for the reheating pass. The diagram illustrates that the first peak did not heat the location of the thermocouple as much as the second one. Although the thermocouple recorded higher temperatures in the second pass, no melting occurred during reheating. It should also be mentioned that the welds were cooled down below 50 °C before applying the laser reheating.

Cross-sections of the four welds are shown in Fig. 3. The laser welding was done with full penetration in conduction mode. Both argon and nitrogen-shielded welds showed the same weld geometry and appearance as the same laser parameters were used. Reheating altered the microstructure of the WM and HAZ but did not affect the weld appearances as no additional melting occurred.

Fig. 2 Thermal cycle recorded by the thermocouple located on the backside of the plate approximately 1.5 mm from the fusion boundary. The welding pass only heated the thermocouple to 600 °C, while the defocused beam used for reheating heated the same location to above 800 °C. The weld was cooled down to below 50 °C before reheating



3.2 Base metal microstructure

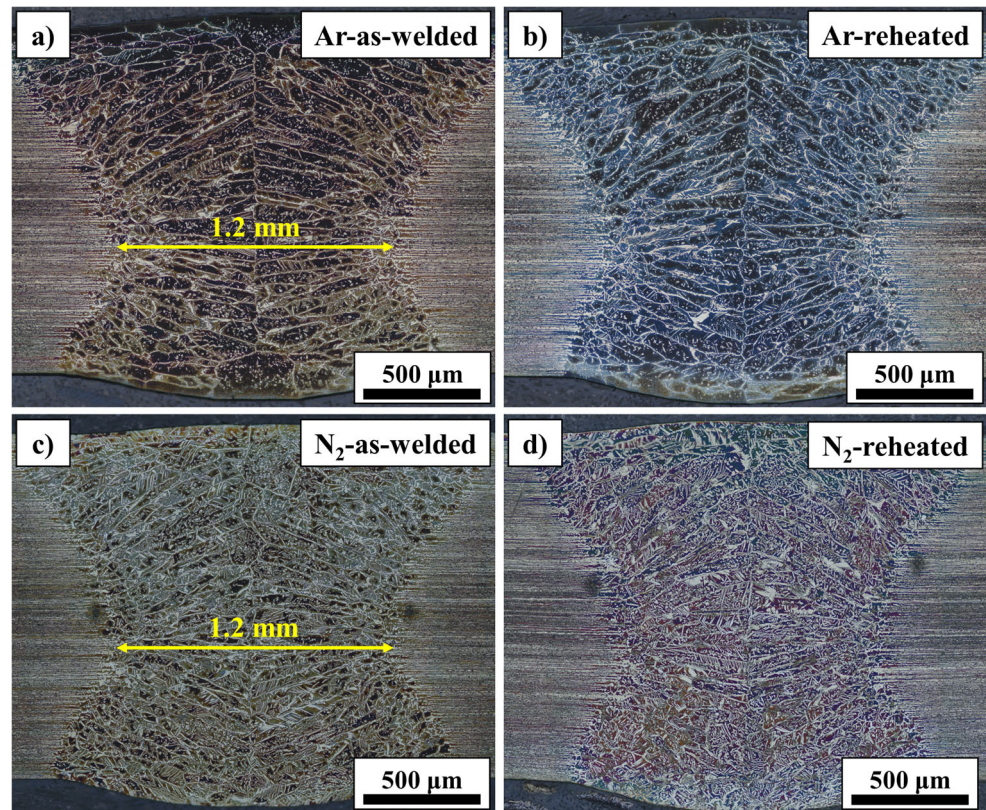
The microstructure of the wrought FDX 27 DSS consisted of ferrite, austenite, and martensite as illustrated in Fig. 4. Measuring the phase fractions by IA gives 36% ferrite. This means it originally contained 64% austenite of which some transformed to martensite either as a result of fabrication or due to surface deformation during sample preparation [31]. It can be noticed that this martensite has an etching response similar to the ferrite when using the Beraha etchant.

3.3 Weld metal microstructure

According to the overall view of the weld in all samples (Fig. 3), epitaxial growth from the fusion line towards the center of the WM can be observed. The austenite fraction increased by using pure nitrogen as shielding and backing gas.

Figure 5 shows the microstructure of the WM at the center of the fusion zone for the two welds in as-welded and reheated conditions. The austenite fractions of the four welds are presented in Fig. 6. As may be seen, by changing the shielding gas from argon to nitrogen, the austenite fraction of the weld increased from 22 to 39% in the as-welded condition. According to Fig. 6, reheating did not affect the austenite fraction in the argon-shielded sample noticeably, but it boosted the austenite fraction to 57% in the N₂-shielded sample. It should be noted that the measured amounts include martensite that has formed either as a result of welding-/reheating-induced stresses or specimen preparation and are therefore representative of the austenite formed at elevated temperatures. The reheated microstructure in nitrogen-shielded condition also underwent growth of primary austenite such as intergranular (grain boundary), Widmannstätten, and intragranular austenite. However, there was no evidence of secondary austenite clusters. Measurement of austenite fractions at the bottom, middle, and top locations of the WM

Fig. 3 Cross-sections of welds: (a) Ar-as-welded, (b) Ar-reheated, (c) N₂-as-welded, and (d) N₂-reheated. Argon and nitrogen shielding produced the same weld geometry (center width: 1.2 mm and area: 2.5 mm²), while nitrogen shielding and reheating resulted in higher austenite fractions. Although a homogeneous bulk and surface austenite distributions can be seen in the N₂-shielded samples, nearly fully ferritic surface regions were found in the argon-shielded samples



confirmed the relatively homogeneous bulk distribution of austenite in the weld zone.

Figure 7 illustrates the microstructure of the as-welded and reheated samples close to the surface. Although the Ar-shielded samples had almost no austenite at the surface, the N₂-shielded sample showed the same level of austenite at the surface as in the bulk. The subsequent reheating also

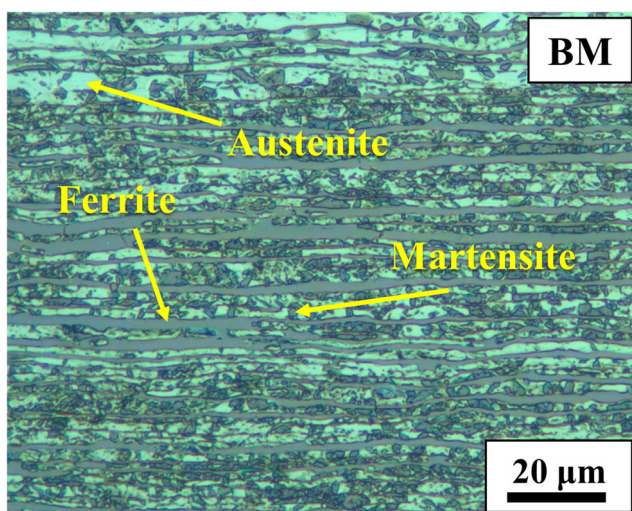


Fig. 4 Microstructure of wrought FDX 27 DSS plate material with ferrite, austenite, and martensite. The martensite etching response is similar to that of ferrite

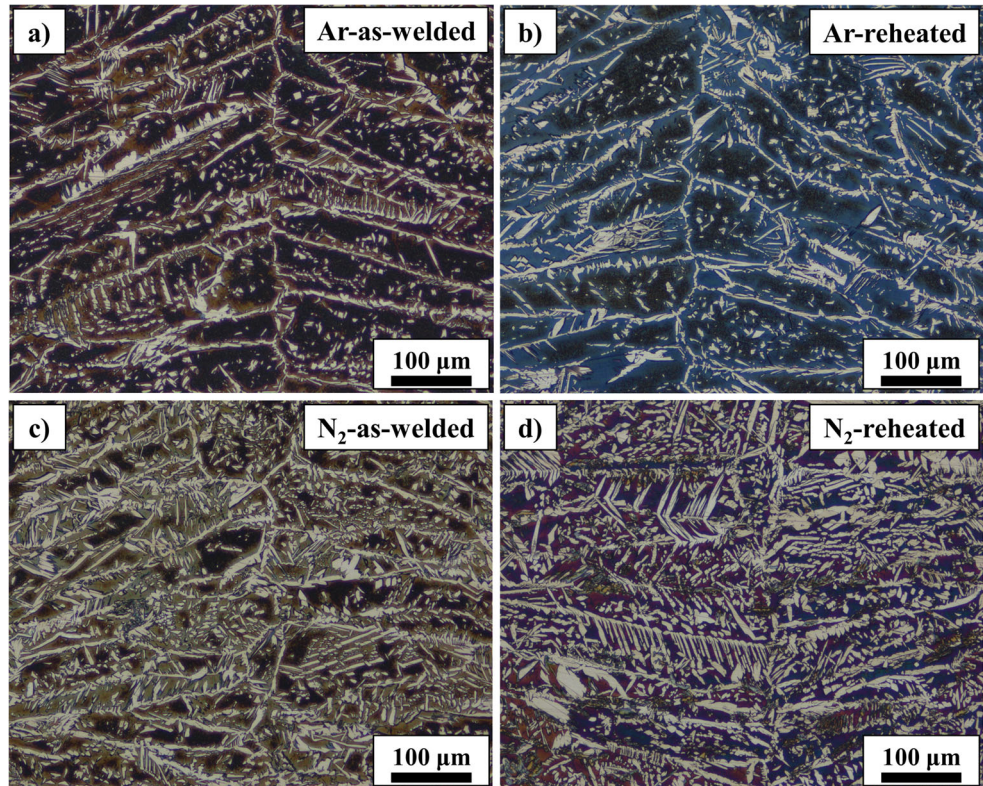
promoted surface austenite formation which was not seen in the Ar-shielded sample.

Higher magnification weld metal micrographs in Fig. 8a and c show nitrides formed during welding. The Ar-shielded weld had larger amounts of nitrides, and using nitrogen as shielding and backing gas mitigated nitride formation. Nitrides were still present in the Ar-reheated sample (Fig. 8b) but were dissolved everywhere in the (surface, center, and root) N₂-reheated sample (Fig. 8d). As discussed earlier, there are also some martensite grains inside the austenite with a similar etching response as the ferrite.

3.4 Heat-affected zone microstructure

The heat-affected zone (HAZ) was also investigated in all four conditions. Figure 9a shows the entire through-thickness HAZ of the Ar-as-welded sample. It is difficult to precisely identify the position of the fusion line in DSS laser welds. However, as the purpose was comparing the effects of argon and nitrogen shielding gas on the HAZ after the laser welding and reheating, the same pattern was used to determine the position of the HAZ in all four samples. The HAZ microstructure can be seen in Fig. 9b at a higher magnification. The HAZ underwent grain growth as a result of the high peak temperature near the fusion boundary. The austenite fractions were measured in the entire HAZ as shown in Fig. 9a, and the results are presented in Fig. 10. The austenite fraction in the

Fig. 5 Microstructure (ferrite, dark; austenite, bright; and martensite, gray) of the weld metal in (a) Ar-as-welded, (b) Ar-reheated, (c) N₂-as-welded, and (d) N₂-reheated conditions. Nitrogen promoted austenite formation during welding as well as reheating



HAZ had a similar behavior as in the WM, such that reheating and changing shielding gas from argon to nitrogen increased the austenite fraction from 33 in the argon-as-welded condition to 59% in the nitrogen-reheated sample.

3.5 Estimation of nitrogen content

As explained in 2.3, a 2-min Gleeble heat treatment at 1100 °C was applied to the WM to provide time for austenite formation reaching a near-equilibrium phase fraction. Fick’s second law was employed to compute the expected

degree of nitrogen diffusion due to the gradient between the WM and the HAZ.

$$\frac{C(x, t) - C_0}{C_s - C_0} = 1 - \text{erf}\left(\frac{x}{\sqrt{Dt}}\right) \text{ (Fick’s second law)}$$

Here t is the diffusion time (2 min), $C(x, t)$ is the nitrogen content at location x and time of t , C_s is the nitrogen content at the fusion boundary ($x = 0$), and C_0 is the initial WM nitrogen content before diffusion. Some assumptions, based on the approach presented in [12], were made such as ferrite being

Fig. 6 Austenite fractions of the WM after laser welding and reheating of FDX 27 DSS with pure argon or pure nitrogen as shielding gas

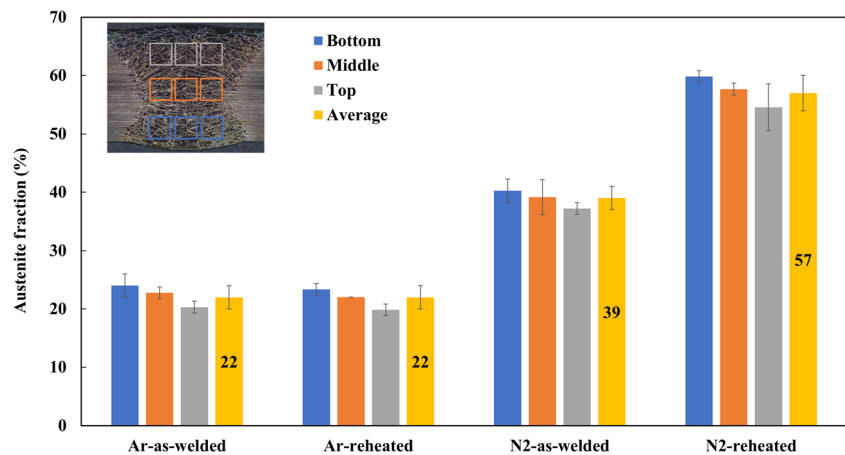


Fig. 7 Microstructure of the weld metal close to the surface showing an almost fully ferritic (dark etching phase) surface region microstructure in (a) Ar-as-welded and (b) Ar-reheated samples. The austenite (white phase) surface fraction in (c) N₂-as-welded and (d) N₂-reheated conditions was very similar to the bulk fraction

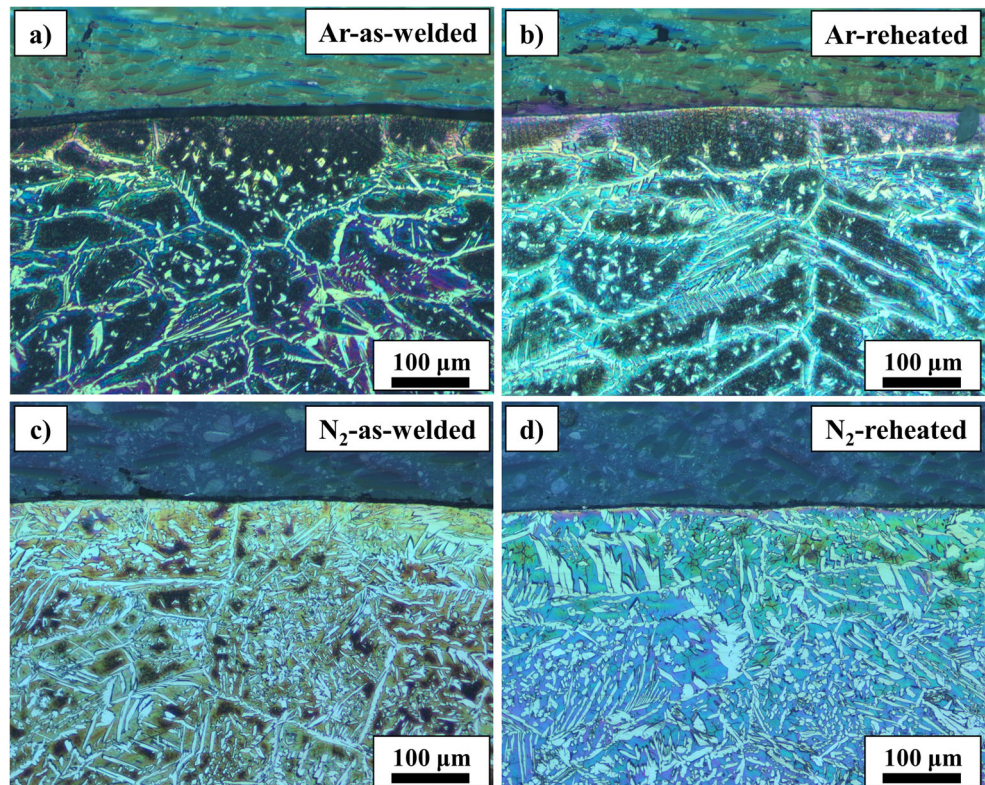
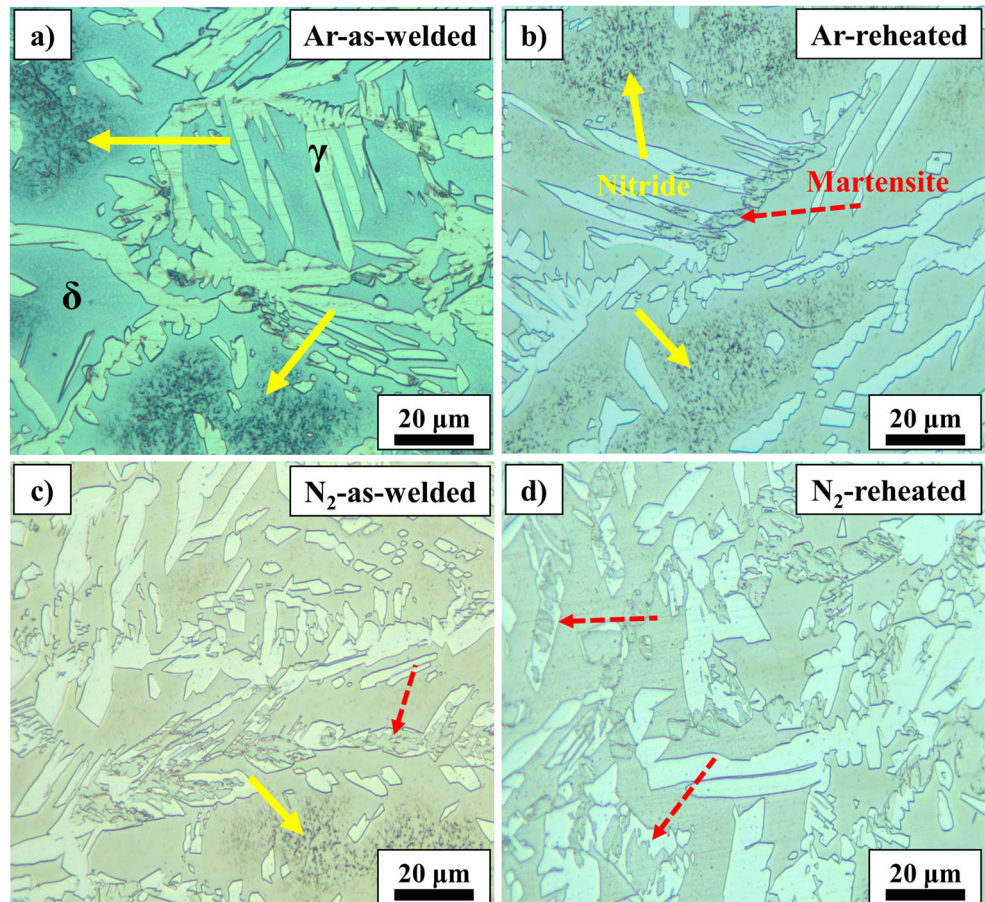


Fig. 8 High magnification light optical micrographs of weld metal microstructures showing nitrides in ferrite and some martensite (red broken arrows) formed in austenite as a result of welding-induced stresses and/or specimen preparation. (a) Ar-as-welded, (b) Ar-reheated, (c) N₂-as-welded, and (d) N₂-reheated. Nitrogen shielding and laser reheating suppressed nitride formation



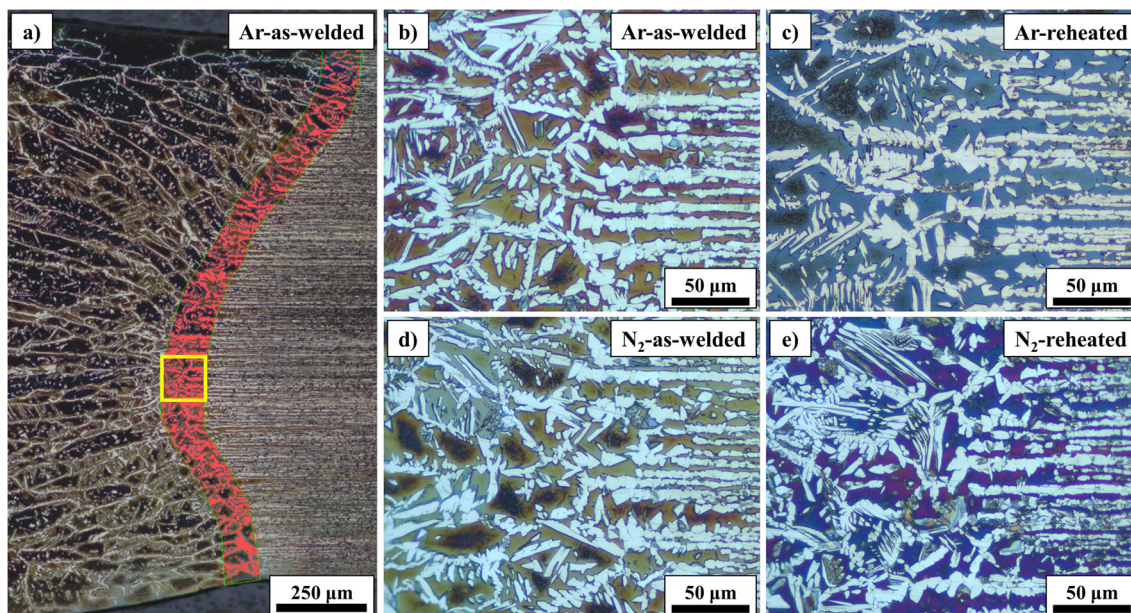


Fig. 9 a The general shape of the HAZ in laser-welded FDX 27 DSS. Higher magnification micrographs of the HAZ microstructure (location shown by yellow square) are shown for (b) Ar-as-welded, (c) Ar-

reheated, (d) N₂-as-welded, and (e) N₂-reheated conditions. Ferrite, austenite, and martensite are dark, bright, and gray, respectively

the only diffusion path. The BM nitrogen content of 0.186 wt.% was used for C_s and a low WM nitrogen content of 0.1 wt.% for C_0 . The diffusion coefficient (D) was computed as $D = D_0 \cdot \exp\left(\frac{-Q}{RT}\right)$, where D_0 , Q , R , and T were $0.47 \text{ mm}^2 \cdot \text{s}^{-1}$, $18,300 \text{ cal} \cdot \text{mol}^{-1}$ (for ferrite), $1,987 \text{ cal} \cdot \text{mol}^{-1} \cdot \text{K}^{-1}$, and 1373 K ($1100 \text{ }^\circ\text{C}$), respectively [32]. The resulting nitrogen concentration profile is shown in Fig. 11a. By relating this diagram to the weld width at plate mid thickness (Fig. 11b), it can be seen that the center of the WM (red broken square) was largely unaffected by nitrogen diffusion. The austenite content in this region can therefore be used for estimation of nitrogen content.

The microstructures at the center of the argon- and nitrogen-shielded WM after Gleeble heat treatment are

illustrated in Figs. 11c, d. The nitrogen contents estimated by comparing the calculated equilibrium phase fractions and phase balance obtained after Gleeble heat treatment at $1100 \text{ }^\circ\text{C}$ are shown in Fig. 12.

The dark blue dashed line represents the nitrogen content of the BM as given in the material producers certificate of 0.186% and the equilibrium austenite fraction computed by Thermo-Calc of around 64%. This is in good agreement with the approximately 64% austenite measured by IA for the BM (see 3.2 and Fig. 4) and illustrates the accuracy of the technique for estimation of nitrogen content. The nitrogen contents of the samples were estimated to be $0.11 \pm 0.01 \text{ wt.}\%$ for Ar-as-welded and $0.16 \pm 0.01 \text{ wt.}\%$ for N₂-as-welded. This indicated a nitrogen loss of around 0.03% in N₂-shielded and 0.08% in Ar-shielded welds as compared to the BM.

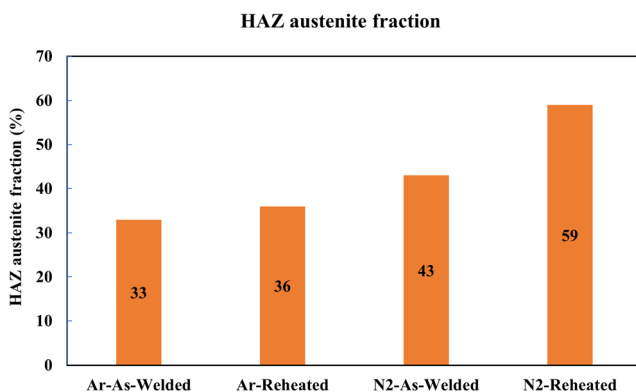


Fig. 10 The heat-affected zone austenite fraction of laser-welded and laser-reheated FDX 27 DSS using pure argon or nitrogen as shielding gas. A clear effect of nitrogen shielding can be seen both in welding and reheating

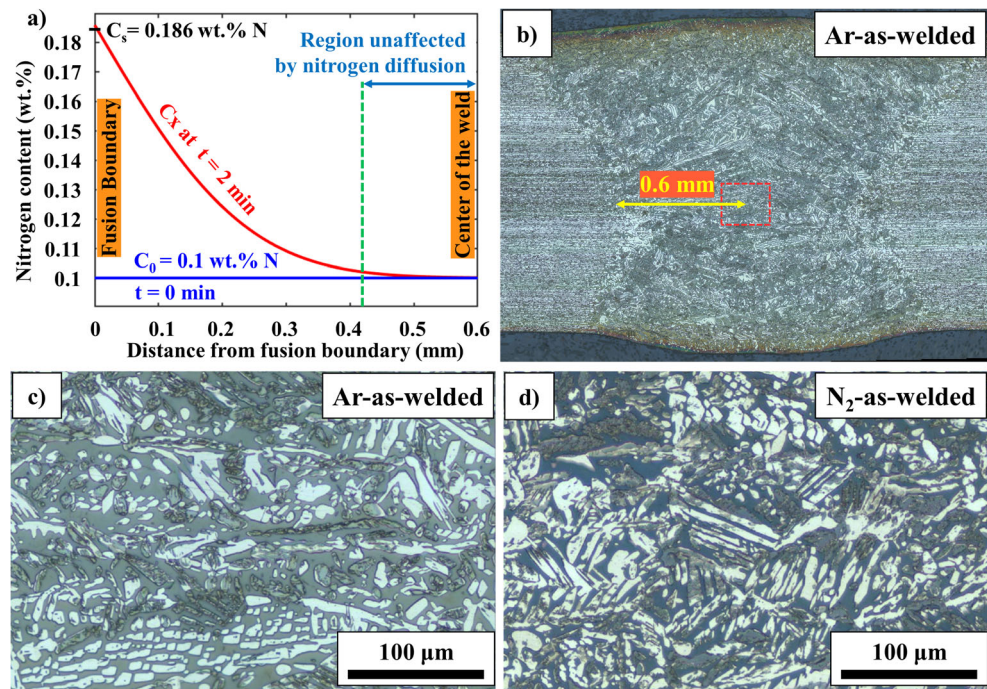
4 Discussion

In this section, welding and laser reheating thermal cycles and their effects on the nitrogen content and microstructure of FDX 27 DSS laser welds are discussed. The main focus is to explain the importance of shielding gas and reheating on the formation of the austenite in the WM and HAZ.

4.1 Thermal cycle and weld profile

The thermal cycles recorded by the thermocouple, located as shown in Fig. 2, demonstrate that the welding cycle did not heat the HAZ as much as the reheating cycle. As the purpose

Fig. 11 (a) Calculated nitrogen concentration profile after 2-min heat treatment at 1100 °C. (b) Weld metal profile and region unaffected by nitrogen diffusion (red broken square). (c) and (d) Microstructure (ferrite, dark; austenite, bright; and martensite, gray) of the WM in Ar-as-welded and N₂-as-welded samples after 2-min Gleeble heat treatment at 1100 °C



of the first pass was welding, the laser beam was focused on the surface of the samples, and consequently, it produced a high-energy density to melt and weld the BM. The aim of the second pass was, on the other hand, reheating without melting. Therefore, the laser was defocused to heat a wider area including the WM and the HAZ but without melting. Although the exact reheating temperature in the weld zone was not measured, it was more than 800 °C based on the recorded peak temperature in the HAZ. In DSS, the temperature range between approximately 800 to 1200 °C is where austenite formation is most rapid [11, 33, 34]. Therefore, the laser

reheating produced the needed temperature cycle for austenite formation.

Investigation of the weld profiles also showed that the weld geometry was dictated by the laser welding parameters, which were the same for argon- and nitrogen-shielded samples. The choice of shielding gas, therefore, did not affect the geometry. Lai et al. [21] investigated the effect of pure argon and nitrogen as well as their mixtures as shielding gas in laser welding of 2205 DSS and observed the same weld geometry regardless of shielding gas. Bauer et al. [35] also indicated that there was no difference between cross-sections of laser-welded DSS shielded by argon and nitrogen with the same welding parameters. In arc welding, in contrast, shielding gas has a significant influence on the weld geometry, since the ionization potential and thermal conductivity of shielding gas can alter both arc shape and melt pool characteristics [36, 37].

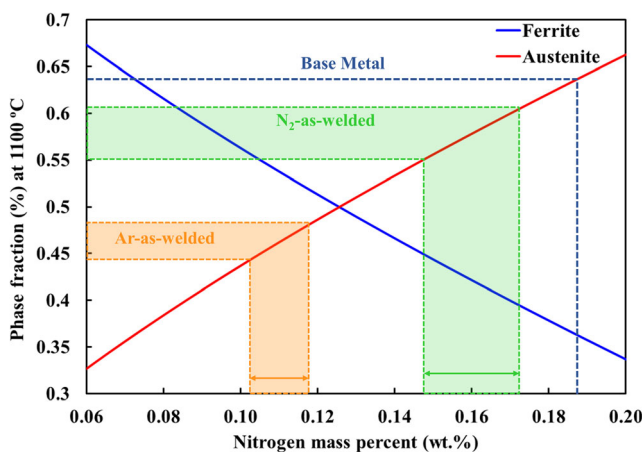


Fig. 12 Equilibrium austenite and ferrite fractions with the variation of nitrogen content at 1100 °C calculated with Thermo-Calc. Weld metal nitrogen contents were estimated by the correlation of measured austenite fraction ranges (46 ± 2 and 58 ± 3) in the Gleeble heat-treated samples with the equilibrium phase fractions of ferrite and austenite at 1100 °C

4.2 Nitrogen loss

To evaluate nitrogen loss, as explained in 2.3 and 3.5, an indirect method was used to estimate the nitrogen content of the weld metal. Compared to the initial nitrogen content of the base metal, both Ar- and N₂-shielded welds showed some nitrogen loss, although significantly more pronounced for Ar-shielded welds. Keskitalo et al. [20] also reported that using nitrogen as shielding gas can to some extent limit the nitrogen loss during laser welding.

Although nitrogen loss affects the phase balance in the bulk of the weld, its influence is most obvious close to the surface

(see Fig. 7). This is of great importance since this will largely dictate corrosion resistance properties [38, 39]. The absence of austenite at the surface in both Ar-as-welded and Ar-reheated samples is also a sign of severe nitrogen loss during laser welding with argon. Nitrogen, however, as the shielding gas, to some extent prevented nitrogen loss such that the surface regions in N₂-as-welded sample had an almost equal amount of austenite as the bulk. As can be observed in Fig. 7, reheating in the presence of nitrogen shielding gas promoted even more austenite formation close to the surface.

4.3 As-welded microstructure

Rapid cooling combined with nitrogen loss can prevent sufficient austenite formation in laser welding of DSS. Nitrogen shielding, in the present study, significantly increased the austenite formation in the as-welded condition compared to argon shielding. As welding was done without a filler metal, nitrogen was the only element differing between the two as-welded conditions. Other studies have pointed out the importance of weld metal nitrogen content for austenite formation [17, 40, 41]. The equilibrium phase fraction diagrams of the two as-welded conditions, calculated by Thermo-Calc, are shown in Fig. 13. As may be seen, the larger nitrogen loss in the argon-shielded weld results in lower equilibrium austenite fractions and delays the beginning of the solid-state transformation of ferrite to austenite after solidification. In addition, faster diffusion at higher transformation temperatures increases growth rate. A higher nitrogen content has therefore, thermodynamically and kinetically, the potential to contribute to the formation of more austenite in the as-welded condition.

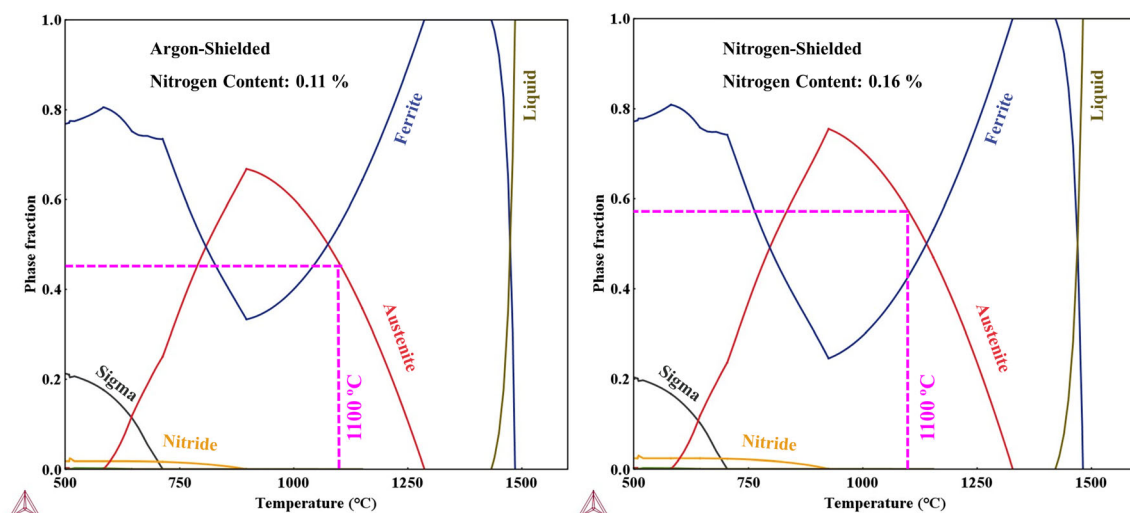


Fig. 13 Equilibrium phase diagrams for the weld metals after experiencing nitrogen loss during laser welding. Nitrogen loss delays austenite formation and decreases the equilibrium fraction of austenite.

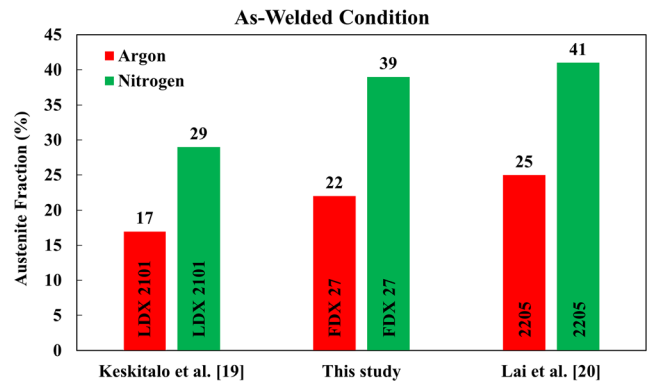


Fig. 14 Comparison of weld metal austenite fractions achieved during fiber laser welding of DSS in different studies. Nitrogen gas shielding promotes austenite formation

According to Fig. 8, by using nitrogen as shielding gas rather than argon, the amount of nitrides was noticeably reduced. The lower nitrogen content of the Ar-as-welded sample pushes the austenite formation start to lower temperatures where diffusion is slower. The lower diffusion rate combined with longer paths due to a lower austenite fraction causes some of the nitrogen to be trapped at some distances from austenite islands. As a result, ferrite becomes saturated in nitrogen which leads to the precipitation of nitrides. The addition of nitrogen via the shielding gas promotes the austenite formation, which can, therefore, significantly decrease the formation of nitrides.

Much research has in recent years focused on the effect of shielding gas on austenite formation during laser welding of DSS. Figure 14 displays a comparison between data from literature [20, 21] and this study. The final austenite fraction of the WM, as pointed out in the introduction, depends on several factors including laser type, laser parameters such as

A higher nitrogen content significantly increases the equilibrium austenite fraction at the 1100 °C heat treatment temperature used for nitrogen content estimation

power, welding speed and spot size, grade of DSS, and its thickness. However, compared to argon, using nitrogen as shielding gas promotes the austenite formation (Table 1). It can also be seen that the same level of austenite fraction can be achieved in the laser-welded FDX 27 DSS as in the more common DSS grade 2205 [21].

4.4 Microstructure in reheated condition

Laser reheating did somewhat unexpectedly not produce any measurable increase of the austenite fraction for the argon-shielded weld. However, the austenite fraction of the nitrogen-shielded weld interestingly increased to 57% from 39%. This change could be attributed to the higher nitrogen content of the N₂-shielded weld. As previously discussed, a low fraction of austenite causes more nitride precipitation, and according to Fig. 8, laser reheating noticeably reduced the fraction of nitrides in the nitrogen-shielded weld. Reheating apparently dissolved nitrides in the ferrite matrix, and the nitrogen from these helped to form more austenite and to approach the equilibrium phase fraction.

Comparing the austenite fractions of the as-welded, laser-reheated, and the Gleeble heat-treated samples demonstrated that for the nitrogen-shielded sample, laser reheating promoted austenite formation to the same level as the Gleeble heat treatment, i.e., 57%. However, laser reheating did not significantly increase the austenite fraction of the argon-shielded sample. The Gleeble heat treatment indicated that the Ar-as-welded sample had the potential to form about $52 \pm 2\%$ austenite at 1100 °C. One reason why the laser reheating did not enhance austenite formation might be that this weld had more or possibly larger nitride particles needing a longer time for dissolution. In addition, as a consequence of the lower austenite content, nitrogen had a longer diffusion path to the austenite (grain boundary, Widmanstätten, and Intragranular), which would delay austenite growth. Further investigations should be performed to demonstrate the effect of these phenomena on the reheating behavior.

As may be seen in Fig. 4, the reheating brings about the growth of primary austenite such as intergranular (grain boundary), Widmannstätten, and intragranular austenite. However, it did not create secondary austenite clusters, which are a typical constituent in the reheated pass of multipass arc-welded components. The reason could be that at high temperatures, the diffusion rate was relatively high, but undercooling promoting nucleation was low, making the growth of primary austenite easier than the nucleation and growth of secondary austenite clusters. Hosseini et al. [33] also observed that the growth of primary austenite was the prominent phenomenon at high temperatures, but the formation of secondary austenite clusters was more favored at lower reheating temperatures in super duplex stainless steel welds. In addition to that, at the

reheating temperatures, secondary austenite precipitation may need a longer time than the reheating period.

4.5 Heat-affected zone microstructure

According to Fig. 7, the HAZ had lower austenite fractions in comparison with the BM. This is related to the rapid cooling and possible nitrogen loss experienced by the HAZ during laser welding. Varbai and Majlinger [42] considered the nitrogen diffusion from HAZ to the WM during welding of DSS. Hosseini et al. [12] also confirmed nitrogen depletion in the HAZ due to high-temperature diffusion and the presence of a nitrogen gradient between the BM and the WM. Similar to the WM, changing the shielding gas from argon to nitrogen increased the HAZ austenite content from 33 to 43%. This can be understood in terms of the higher nitrogen content in the N₂-as-welded sample creating a smaller concentration gradient causing nitrogen diffusion from HAZ into the WM. Also similar to the weld metal behavior, reheating did not significantly affect the austenite content in the HAZ of the argon-shielded sample but increased HAZ austenite content of the nitrogen-shielded sample. As in the WM, laser reheating dissolved nitrides in the nitrogen-shielded sample HAZ and allowed nitrogen to diffuse and the system to move towards equilibrium.

5 Conclusions

The effects of using pure argon or nitrogen as shielding and backing gas and that of laser reheating were investigated in laser welding of 1.5-mm-thick FDX 27 DSS. Characterization of microstructures, measurements of austenite fractions, and thermodynamic calculations demonstrated how shielding gas and laser reheating contribute to austenite formation.

- 1- The as-welded austenite fraction increased from 22 to 39% when changing the shielding and backing gas from pure argon to pure nitrogen.
- 2- Laser reheating increased the austenite fraction from 39 to 57% for the N₂-shielded weld but did not have any measurable effects when using Ar shielding.
- 3- The HAZ austenite fractions followed the WM trends with a maximum austenite fraction of 59% in the reheated nitrogen-shielded sample.
- 4- An almost fully ferritic microstructure was seen at the surface of Ar-shielded samples, while the N₂-shielded samples had an acceptable distribution of austenite also at the surface.
- 5- Nitrides were observed in WM and HAZ for both Ar- and N₂-shielding, but the amount was lower with N₂-shielding. Laser reheating produced a largely nitride-free microstructure in the N₂-shielding weld.

- 6- Nitrogen contents of weld metals were evaluated from calculated equilibrium phase diagrams and measured austenite fractions after equilibrating heat treatments at 1100 °C. The estimated contents were 0.16% for N₂-shielded and 0.11% for Ar-shielded welds, as compared to 0.186% for the base metal.
- 7- Applying nitrogen as shielding gas in laser welding of DSS followed by subsequent laser reheating can notably promote austenite formation and suppress nitride precipitation.

Acknowledgments Open access funding provided by University West. James Oliver and Ravi Vishnu from the Outokumpu Stainless AB (Avesta, Sweden) are appreciatively acknowledged for their help and support. This study received great support from the EU-project H2020-MSCA-RISE-2018 Number 823786, i-Weld, and the Swedish Agency for Economic and Regional Growth through the European Union – European Development Fund.

Compliance with ethical standards

Conflict of interest The authors declare that they have no conflict of interest.

Open Access This article is licensed under a Creative Commons Attribution 4.0 International License, which permits use, sharing, adaptation, distribution and reproduction in any medium or format, as long as you give appropriate credit to the original author(s) and the source, provide a link to the Creative Commons licence, and indicate if changes were made. The images or other third party material in this article are included in the article's Creative Commons licence, unless indicated otherwise in a credit line to the material. If material is not included in the article's Creative Commons licence and your intended use is not permitted by statutory regulation or exceeds the permitted use, you will need to obtain permission directly from the copyright holder. To view a copy of this licence, visit <http://creativecommons.org/licenses/by/4.0/>.

References

1. Gunn RN (1997) Duplex stainless steels: microstructure, properties and applications. Woodhead Publ 5:12
2. Messer B, Oprea V, Wright A (2007) Duplex stainless steel welding: best practices. *Stainl Steel World* (December 2007) :53–63
3. Salminen A, Westin EM (2010) Effect of heat input modification on duplex stainless weld quality. 29th Int Congr Appl Lasers Electro-Optics, ICALEO 2010 - Congr Proc 103:668–675. <https://doi.org/10.2351/1.5062097>
4. Vänskä M, Salminen A (2012) Laser welding of stainless steel self-steering tube-to-tube joints with oscillating mirror. *Proc Inst Mech Eng Part B J Eng Manuf* 226:632–640. <https://doi.org/10.1177/0954405411425114>
5. Karlsson L, Arcini H (2012) Low energy input welding of duplex stainless steels. *Weld World* 56:41–47
6. Omura T, Kushida T, Komizo Y (2000) Microstructural features and corrosion properties in laser welded duplex stainless steels. *Weld Int* 14:257–260. <https://doi.org/10.1080/09507110009549176>
7. Hänninen H, Romu J, Ilola R, Tervo J, Laitinen A (2001) Effects of processing and manufacturing of high nitrogen-containing stainless steels on their mechanical, corrosion and wear properties. *J Mater Process Technol* 117:424–430
8. Li J, Ma Z, Xiao X, Zhao J, Jiang L (2011) On the behavior of nitrogen in a low-Ni high-Mn super duplex stainless steel. *Mater Des* 32:2199–2205
9. Lippold JC, Kotecki DJ, Sant S (2006) Welding metallurgy and weldability of stainless steels. *MRS Bull Res Soc* 31:58
10. Park YH, Lee ZH (2001) Effect of nitrogen and heat treatment on the microstructure and tensile properties of 25Cr-7Ni-1.5Mo-3W-xN duplex stainless steel castings. *Mater Sci Eng A* 297:78–84. [https://doi.org/10.1016/S0921-5093\(00\)01263-6](https://doi.org/10.1016/S0921-5093(00)01263-6)
11. Hosseini VA, Wessman S, Hurtig K, Karlsson L (2016) Nitrogen loss and effects on microstructure in multipass TIG welding of a super duplex stainless steel. *Mater Des* 98:88–97. <https://doi.org/10.1016/j.matdes.2016.03.011>
12. Hosseini VA, Karlsson L (2019) Physical and kinetic simulation of nitrogen loss in high temperature heat affected zone of duplex stainless steels. *Materialia* 6:100325. <https://doi.org/10.1016/j.mtla.2019.100325>
13. Nowacki J, Lukojc A (2006) Microstructural transformations of heat affected zones in duplex steel welded joints. *Mater Charact* 56:436–441
14. Chen TH, Yang JR (2002) Microstructural characterization of simulated heat affected zone in a nitrogen-containing 2205 duplex stainless steel. *Mater Sci Eng A* 338:166–181
15. Valiente Bermejo MA, Karlsson L, Svensson LE, Hurtig K, Rasmuson H, Frødigh M, Bengtsson P (2014) Effect of shielding gas on welding performance and properties of duplex and superduplex stainless steel welds. *Weld World* 59:239–249. <https://doi.org/10.1007/s40194-014-0199-7>
16. Sathiya P, Aravindan S, Soundararajan R, Noorul Haq A (2009) Effect of shielding gases on mechanical and metallurgical properties of duplex stainless-steel welds. *J Mater Sci* 44:114–121. <https://doi.org/10.1007/s10853-008-3098-8>
17. Kim ST, Jang SH, Lee IS, Park YS (2011) Effects of solution heat-treatment and nitrogen in shielding gas on the resistance to pitting corrosion of hyper duplex stainless steel welds. *Corros Sci* 53:1939–1947. <https://doi.org/10.1016/j.corsci.2011.02.013>
18. Yang Y, Wang Z, Tan H, Hong J, Jiang Y, Jiang L, Li J (2012) Effect of a brief post-weld heat treatment on the microstructure evolution and pitting corrosion of laser beam welded UNS S31803 duplex stainless steel. *Corros Sci* 65:472–480. <https://doi.org/10.1016/j.corsci.2012.08.054>
19. Westin EM, Fellman A (2010) Effect of laser and laser hybrid welding on the corrosion performance of a lean duplex stainless steel. *J Laser Appl* 22:150–158. <https://doi.org/10.2351/1.3533146>
20. Keskitalo M, Mäntyjärvi K, Sundqvist J, Powell J, Kaplan AFH (2015) Laser welding of duplex stainless steel with nitrogen as shielding gas. *J Mater Process Technol* 216:381–384. <https://doi.org/10.1016/j.jmatprotec.2014.10.004>
21. Lai R, Cai Y, Wu Y, Li F, Hua X (2016) Influence of absorbed nitrogen on microstructure and corrosion resistance of 2205 duplex stainless steel joint processed by fiber laser welding. *J Mater Process Technol* 231:397–405. <https://doi.org/10.1016/j.jmatprotec.2016.01.016>
22. Capello E, Chiarello P, Previtali B, Vedani M (2003) Laser welding and surface treatment of a 22Cr-5Ni-3Mo duplex stainless steel. *Mater Sci Eng A* 351:334–343. [https://doi.org/10.1016/S0921-5093\(02\)00841-9](https://doi.org/10.1016/S0921-5093(02)00841-9)
23. Salminen A, Westin E, Lappalainen E, Unt A (2012) Effect of gas shielding and heat input on autogenous welding of duplex stainless steel, ICALEO 2012 - 31st. Int Congr Appl Lasers Electro-Optics 524:524–531. <https://doi.org/10.2351/1.5062503>
24. Saravanan S, Raghukandan K, Sivagurumanikandan N (2017) Pulsed Nd: YAG laser welding and subsequent post-weld heat

- treatment on super duplex stainless steel. *J Manuf Process* 25:284–289. <https://doi.org/10.1016/j.jmapro.2016.12.015>
25. Young MC, Tsay LW, Shin CS, Chan SLI (2007) The effect of short time post-weld heat treatment on the fatigue crack growth of 2205 duplex stainless steel welds. *Int J Fatigue* 29:2155–2162. <https://doi.org/10.1016/j.ijfatigue.2007.01.004>
 26. Rahman Rashid RA, Nazari KA, Barr C, Palanisamy S, Orchowski N, Matthews N, Dargusch MS (2019) Effect of laser reheat post-treatment on the microstructural characteristics of laser-cladded ultra-high strength steel. *Surf Coat Technol* 372:93–102. <https://doi.org/10.1016/j.surfcoat.2019.05.021>
 27. Kolenič F, Kovac L, Drimal D (2011) Effect of laser welding conditions on austenite/ferrite ratio in duplex stainless steel 2507 welds. *Weld World* 55:19–25. <https://doi.org/10.1007/BF03321292>
 28. Tian Y, Lin S, Ko JYP, Lienert U, Borgenstam A, Hedström P (2018) Micromechanics and microstructure evolution during in situ uniaxial tensile loading of TRIP-assisted duplex stainless steels. *Mater Sci Eng A* 734:281–290. <https://doi.org/10.1016/j.msea.2018.07.040>
 29. Choi JY, Ji JH, Hwang SW, Park KT (2012) Effects of nitrogen content on TRIP of Fe-20Cr-5Mn-xN duplex stainless steel. *Mater Sci Eng A* 534:673–680. <https://doi.org/10.1016/j.msea.2011.12.025>
 30. Hosseini VA, Hurtig K, Eyzop D, Östberg A, Janiak P, Karlsson L (2019) Ferrite content measurement in super duplex stainless steel welds. *Weld World* 63:551–563. <https://doi.org/10.1007/s40194-018-00681-1>
 31. Jiang S-y, Wang Y, Xing X-d, Zhang Y-q (2020) Stress-induced martensite phase transformation of FeMnSiCrNi shape memory alloy subjected to mechanical vibrating polishing. *Trans Nonferrous Met Soc China (English Ed)* 30:1582–1593. [https://doi.org/10.1016/S1003-6326\(20\)65321-3](https://doi.org/10.1016/S1003-6326(20)65321-3)
 32. Bobadilla M, Tschiptschin A (2015) On the nitrogen diffusion in a duplex stainless steel. *Mater Res* 18:390–394. <https://doi.org/10.1590/1516-1439.337714>
 33. Hosseini VA, Karlsson L, Engelberg D, Wessman S (2018) Time-temperature-precipitation and property diagrams for super duplex stainless steel weld metals. *Weld World* 62:517–533. <https://doi.org/10.1007/s40194-018-0548-z>
 34. Zhang L, Zhang W, Jiang Y, Deng B, Sun D, Li J (2009) Influence of annealing treatment on the corrosion resistance of lean duplex stainless steel 2101. *Electrochim Acta* 54:5387–5392. <https://doi.org/10.1016/j.electacta.2009.04.023>
 35. Bauer B, Topić A, Kralj S, Kožuh Z (2011) Influence of the gas composition on the geometry of laser-welded joints in duplex stainless steel. *Mater Tehnol* 45:413–419
 36. Rodrigues A, Loureiro A (2005) Effect of shielding gas and activating flux on weld bead geometry in tungsten inert gas welding of austenitic stainless steels. *Sci Technol Weld Join* 10:760–765. <https://doi.org/10.1179/174329305X68769>
 37. Hertzman S, Wessman S (1999) An experimental and theoretical study of nitrogen flux in stainless steel TIG welds. *Mater Scie Forum* 318–320:579–590. <https://doi.org/10.4028/www.scientific.net/msf.318-320.579>
 38. Tavares SSM, Pardal JM, Lima LD, Bastos IN, Nascimento AM, de Souza JA (2007) Characterization of microstructure, chemical composition, corrosion resistance and toughness of a multipass weld joint of superduplex stainless steel UNS S32750. *Mater Charact* 58:610–616. <https://doi.org/10.1016/j.matchar.2006.07.006>
 39. Tan H, Jiang Y, Deng B, Sun T, Xu J, Li J (2009) Effect of annealing temperature on the pitting corrosion resistance of super duplex stainless steel UNS S32750. *Mater Charact* 60:1049–1054. <https://doi.org/10.1016/j.matchar.2009.04.009>
 40. Hertzman S, Pettersson RJ, Blom R, Kivineva E, Eriksson J (1996) Influence of shielding gas composition and welding parameters on the n-content and corrosion properties of welds in n-alloyed stainless steel grades. *ISIJ Int* 36:968–976. <https://doi.org/10.2355/isijinternational.36.968>
 41. Matsunaga H, Sato YS, Kokawa H, Kuwana T (1998) Effect of nitrogen on corrosion of duplex stainless steel weld metal. *Sci Technol Weld Join* 3:225–232
 42. Varbai B, Májlinger K (2019) Physical and theoretical modeling of the nitrogen content of duplex stainless steel weld metal: shielding gas composition and heat input effects. *Metals (Basel)* 9:762. <https://doi.org/10.3390/met9070762>

Publisher's note Springer Nature remains neutral with regard to jurisdictional claims in published maps and institutional affiliations.